Available online at www.sciencedirect.com
ScienceDirect
Acta Materialia 55 (2007) 3593–3600
Acta MATERIALIA
www.elsevier.com/locate/actamat

Stress-induced martensitic phase transformation in thin sheets of Nitinol

S. Daly, G. Ravichandran, K. Bhattacharya *

Division of Engineering and Applied Science, California Institute of Technology, Pasadena, CA 91125, USA

Received 13 September 2006; received in revised form 7 February 2007; accepted 8 February 2007
Available online 6 April 2007

Abstract

Using the *in situ* optical technique known as digital image correlation (DIC), full-field quantitative strain maps of localization have been experimentally obtained for the first time in thin sheets of Nitinol. The use of DIC provides new information connecting previous observations on the micro- and macro-scales. It shows that the transformation initiates before the formation of localized bands, and the strain inside the bands does not saturate when they nucleate. The effect of rolling texture on the macroscopic stress–strain behavior was observed and it is shown that the resolved stress criterion or Clausius–Clapeyron relation does not hold for polycrystalline Nitinol. Finally, the effect of geometric defects on localization behavior was observed.

Keywords: Phase transformation; Shape-memory alloys; Texture

1. Introduction

Shape-memory alloys (SMAs) have the ability to return to a previously defined shape when heated past a set transformation temperature following deformation. Many SMAs also display superelastic or pseudoelastic behavior where large deformation can be recovered on unloading. These properties make SMAs, and in particular nickel–titanium (Nitinol), attractive for a variety of applications. Important amongst these are stents, guidewires and other biomedical applications in which relatively slender structures are subjected to rather complex deformations. These applications are the motivation for understanding the deformation mechanism in these materials. Of particular interest is the propensity of these materials to form localized bands of large strain.

The deformation is recovered in these materials because it is accommodated by martensitic phase transformation and transformation twinning/detwinning rather than by crystallographic slip [1,2]. These materials undergo a martensitic phase transformation from a high-temperature, high-symmetry austenite state to a low-temperature, low-symmetry martensite state. The change of symmetry gives rise to multiple variants of martensite which can form transformation twins. Superelastic behavior arises when the material is deformed at a temperature sufficiently above the transformation temperature. The stress-induced austenite to martensite transformation gives rise to the deformation on loading. However, the martensite is unstable at this temperature and transforms back to the austenite on unloading, thereby recovering the deformation. The mechanism of transformation is reasonably well understood in single crystals (see e.g. Ref. [23] and references therein), but incompletely understood in polycrystals.

Leo et al. [5] and Shaw and Kyriakides [6] studied stress-induced transformation in polycrystalline nickel–titanium wires, and observed that the transformation proceeded through the nucleation and propagation of regions of large strain. Subsequently, Shaw and Kyriakides [7] observed the formation of Lüders-like bands in these materials. Since then strain localization has been much investigated, both experimentally and theoretically [8–14], for the inherent scientific interest of such materials and also for their applications in medical devices. However, no measurements of the

* Corresponding author. Tel.: +1 626 395 8306.
E-mail address: bhatta@caltech.edu (K. Bhattacharya).

1359-6454/$30.00
doi:10.1016/j.actamat.2007.02.011

strain and its evolution during deformation have been reported.

In this paper, we present full-field measurements of the strain during stress-induced martensitic phase transformations of thin sheets of Nitinol subjected to uniaxial tension. These measurements were obtained by digital image correlation (DIC), an in situ optical method that measures displacement on the surface of an object by tracking and correlating a random pattern on the sample surface [15]. Our observations show that the progress of the transformation is much more complex than commonly assumed. The transformation initiates before the nucleation of bands. It is not complete within the bands on nucleation, but proceeds with increasing load. The transformation is not complete even upon apparent saturation. We examine the role of texture by extracting specimens with different orientations with respect to the rolling direction (RD). We also examine the role of geometric defects on localization.

2. Materials and experimental details

Dog-bone shaped tensile specimens as shown in Fig. 1 were extracted by wire electrical discharge machining from rolled sheets with a nominal thickness of 160 μm and a composition of 48 wt.% Ti and 52 wt.% Ni. The sheets were flat annealed at an A_f temperature of 11.3 °C. The low A_f ensured that the specimens were fully austenitic when unloaded and that stress-induced martensite occurred upon loading.

Tensile specimens with varying orientations with respect to the RD were extracted from the same sheet. To understand the texture of the rolled sheet, optical micrographs of the tensile specimens were obtained by heavily etching them in $1HF + 4HNO_3 + 5H_2O$ for 30–45 s. This recipe was adapted from work done by Shabalovskaya et al. [16]. The results are shown in Fig. 2 for three specimens numbered 1–3, oriented along the RD, perpendicular to RD, and 45° to RD, respectively. The micrographs show elongated etch pits in the RD underscoring the texture. Further, the three micrographs are very similar except for orientation, demonstrating the homogeneity of the rolled sheet. Finally, these, and more lightly etched specimens, demonstrate that the grain size in this rolled sheet is of the order of 100 nm.

The specimens were tested in uniaxial tension under displacement control using a computer-controlled servo-hydraulic machine (MTS Model No. 358.10). Knurled grips were used to minimize slippage and were carefully aligned to minimize out-of-plane loading and displacement. Grip slippage was also minimized by attaching emery paper to the grip sections of the sample in order to maximize friction in the connection between the grips and the sample. Specimens were tested with a fixed bottom grip and moving upper grip, both of which were supported by pivots to minimize bending and shear in the specimens. The applied strain rate was $10^{-3}\,s^{-1}$. This is somewhat higher than the $10^{-4}\,s^{-1}$ recommended by various researchers for ideal isothermal tests, but was found to be adequate for our thin sheets and enabled the variety of observations that we conducted.

The strain in the specimen was measured using DIC. This is an in situ optical correlation method used to measure displacement on the surface of an object by tracking a random pattern on the sample surface. The random pattern could be inherent surface features or an artificially applied pattern, but must provide a sizeable number of correlation points at the magnification of imaging. In this experiment, the pattern was applied pre-test by first coating the sample in white paint and then spraying a light mist of black paint in a fine speckle pattern. Images were recorded using a 1200×1600 CCD camera focused on the specimen surface and linked to a computer for data acquisition. Up to three lenses were used to focus the image, depending on the area of interest; a 50 mm Nikon was used as the main lens, and two Sigma ×2 and Sigma ×1.4 lenses were also utilized for zooming purposes. Since the deformation was in-plane, a single CCD camera could be used to capture the deformation. Images were taken after each displacement increment and post-processing was achieved with the software Vic-2D developed by Correlated Solutions (www.correlatedsolutions.com) to extract the strain fields.

There are certain sources of error in these experiments that need to be discussed briefly. There is grip slippage, although testing for the stability of MTS applied force pre-test helped to minimize this error. There is grip alignment error, which was minimized by carefully aligning the grips and checking alignment with each experiment, and the self-aligning nature of the grip. There are also analysis errors due to any out-of-plane deformation of the specimen. There are numerous parameters in the Vic-2D Correlated Solutions program that can be adjusted, and these parameters have a significant effect on the success

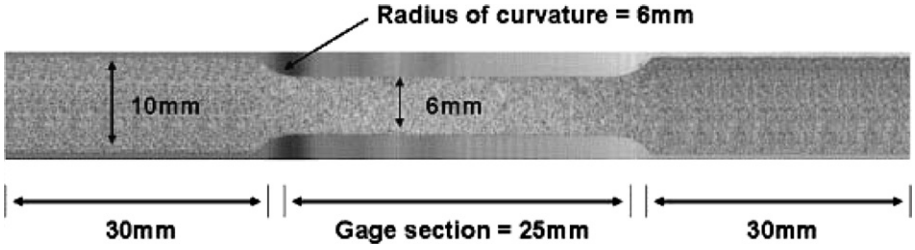

Fig. 1. Specifications of the dog-bone test specimens.

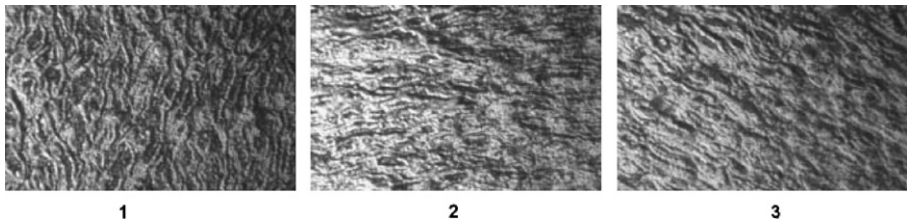

Fig. 2. Optical micrograph of NiTi sheet at 60× at three different orientations: (1) parallel to RD, (2) 45° to RD and (3) perpendicular to RD.

of the computation. Improper lighting, dust, marks on the camera lens, inadequate camera shutter speed, or inadequate aperture speed can produce a faulty or blurred speckle pattern and cause failure. With our specifications and settings, we estimate the strain accuracy to be approximately 0.1%.

3. Experimental observations

3.1. Uniaxial tension parallel to the rolling direction

Fig. 3 presents a detailed progression of the mesoscopic and macroscopic stress–strain behavior of a dog-bone specimen cut parallel to the RD and subjected to uniaxial tension under displacement control. Snapshots of the specimen were taken after each displacement increment, and the strain distributions were computed. The overall strain of the specimen in the longitudinal direction is obtained from the average of the strain over the entire specimen. This was verified by extensometer and strain gages. This overall axial strain is plotted against the nominal stress applied by the MTS machine in Fig. 3. The pictures that accompany the macroscopic stress–strain curve show the evolution of the normal component of strain in the longitudinal direction. The unloading curve was recalibrated and adjusted downwards to compensate for the offset in the MTS loading frame.

The specimen is fully austenitic at the beginning of the test, and behaves in a linear elastic manner with an approximate modulus of 45 GPa. It begins to deviate from linearity with an apparent drop of modulus around a stress of 460 MPa and strain of 1%. The accompanying image shows that the strain is almost but not completely uniform throughout the specimen. As the loading continues, the level of strain continues to increase throughout the specimen, until we begin to see the appearance of a localized band of high strain close to the bottom grip at around 1.5% strain. Further deformation occurs by the broadening and nucleation of new bands with little apparent increase of stress. The bands are all parallel in this specimen and oriented at approximately 55° from the loading axis. The bands gradually coalesce and the stress begins to increase around a macroscopic strain of 4.25%. A short transition follows and the behavior becomes linear beyond that point with a modulus of approximately 15 GPa.

The unloading follows a similar pattern. It begins with an almost linear unloading with a modulus of approximately 30 GPa. There is a departure from linearity at about 4% strain, and the first localized band with small strain appears around 2.8% strain. The subsequent decrease in

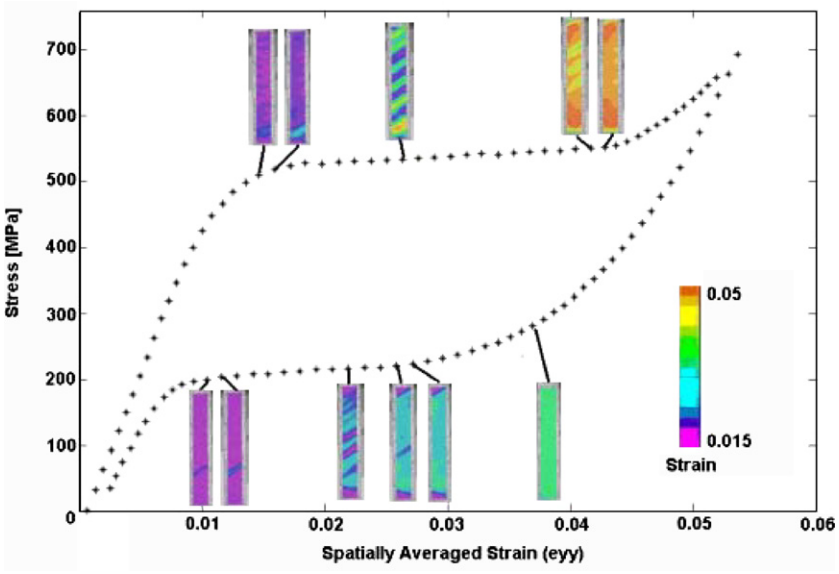

Fig. 3. The macroscopic response of a dog-bone specimen cut parallel to the RD with corresponding DIC images. The macroscopic response is the spatially averaged strain value from each DIC image plotted vs. the MTS stress value.

strain is caused by the growth of nucleation of new bands with little apparent decrease of stress. The bands eventually coalesce and this is followed by linear unloading. There is a small amount of residual strain, as is expected for any virgin specimen.

For future use, we label the stress at which we see deviation from linearity on loading as the transformation onset stress (σ_T), and the residual strain that would be obtained if the unloading were purely linear as the transformation strain (ε_T).

Fig. 4 shows the longitudinal strain along the centerline of the sample at three points during the loading phase, prior to the appearance of any macroscopic localization, halfway through the transformation when all the bands have nucleated and are nominally halfway through growing, and immediately after the coalescence of the bands with no remaining localization.

Note that the strain levels are quite high, above 1.2%, before there is any macroscopic localization. Further, note that the strain is not perfectly uniform but suffers from small fluctuations. Once localization begins, the value of the strain inside the band does not jump directly to the maximum (saturation) level. Instead, it gradually increases even as the bands grow. Finally, once the band coalesces at the end of localization, the strain is almost, but not perfectly, uniform throughout the specimen.

3.2. Uniaxial tension in various orientations

Fig. 5 shows the macroscopic stress–strain behavior under uniaxial tension of dog-bone specimens cut out of the same sheet, but at various orientations relative to the RD. As before, a photograph of the specimen is taken after each displacement increment, and this image is used to calculate the strain field. The macroscopic strain is obtained by averaging. The qualitative behavior is very similar to that described above. It begins linearly, with a deviation

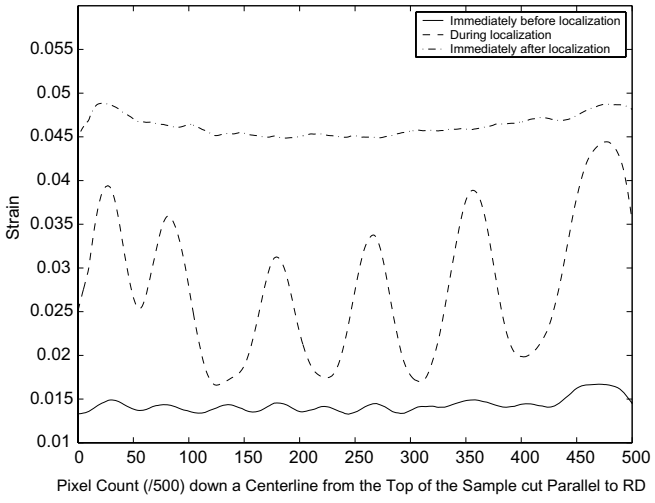

Fig. 4. Strain down the centerline of a dog-bone specimen cut parallel to the RD during various localization stages.

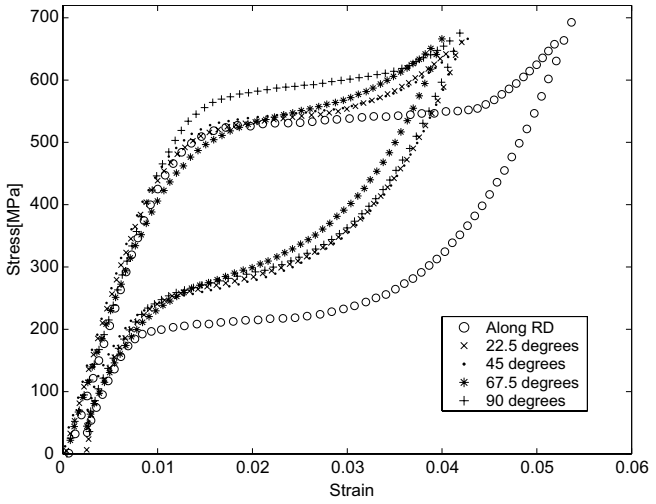

Fig. 5. The uniaxial stress–strain response of various specimens with different orientations to the RD.

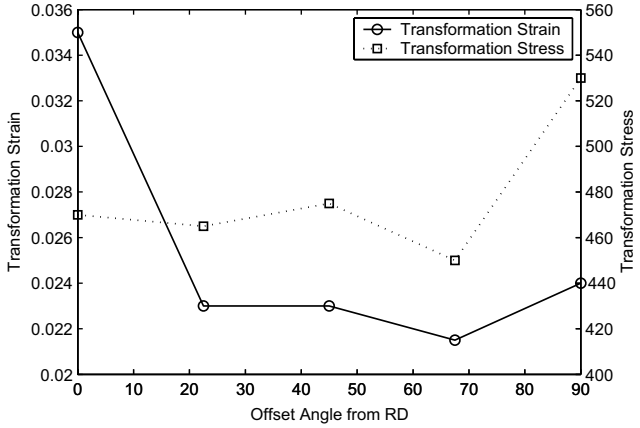

Fig. 6. The variation of transformation initiation stress and transformation strain with orientation.

and associated small oscillations in strain from linearity at 1% strain, the appearance of localized bands of strain at approximately 1.5% strain accompanied by a plateau in the stress–strain curve, growth of the bands and growth of the strain in the bands until coalescence, followed by a rising stress–strain curve, and a similar pattern on unloading. However, the transformation onset stress and transformation strain depend on orientation. The transformation strain decreases as we move away from the RD, reaching a minimum at 67.5° and then recovering a little. The transformation onset stress is approximately the same for all orientations, except for specimens cut at 90° to the RD. The observed localization patterns and the evolution of strain is similar.

The same experiment was repeated in specimens cut from various sheets obtained from the same manufacturer. The characteristics of the macroscopic stress–strain curves were very similar, with a variation in transformation onset stress and transformation strains <25% from

sheet to sheet. However, the localization in some specimens showed a crossing pattern, as shown in Fig. 7, with both sets of bands oriented at approximately 55° to the loading axis.

The same experiment was also repeated in the same specimen multiple times, including removing the specimen from the loading frame and then remounting it. The results, specifically the stress–strain curve and localization patterns, were repeatable except for the small residual strain in the first few cycles.

3.3. Strain fields around surface features

To understand the origin of the strain localization and the sensitivity to defects, the above experiments were also repeated in specimens with holes and side notches.

3.3.1. Surface feature: hole

Dog-bone specimens oriented along the rolling axis were prepared with a 1 mm hole centered biaxially in the gage region. Observations of strain were at low-magnification with the entire specimen in the field of view, and repeated at high-magnification close to the hole. Fig. 8 shows the results of these experiments in separate specimens for the low- and high-magnification so that both sets show the results for a virgin specimen. The macroscopic stress–strain behavior is similar to that observed earlier. As expected, we see larger strains in the immediate vicinity of the hole, and two bands of localized strain in a crossing pattern nucleates from there. Once again, the strains in these bands are less than the fully saturated values when these bands first form, and gradually increase with increasing loading. The bands also increase in size. As the loading continues to increase, other bands oriented approximately 55° to the loading axis form in the regular portions of the gage section.

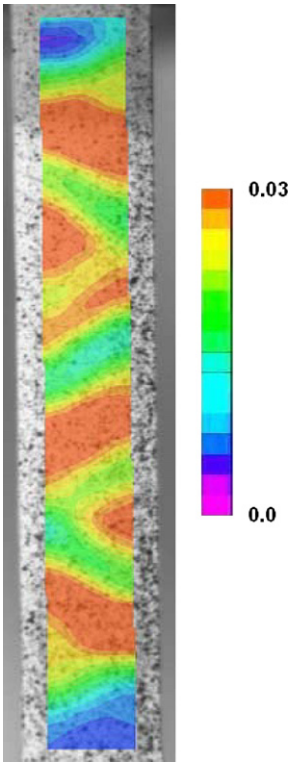

Fig. 7. An example of the crossing bands found in some specimens.

The high-resolution images provide further insight into the development of the strains. It is important, however, to note that DIC is unable to resolve the strains in a small annulus around the hole. It is therefore possible, and indeed likely, that there is increased strain at some points in this annulus. Two small regions of increased strain adjacent to the hole become visible and develop into kidney-shaped lobes in Fig. 8-1. These lobes are reminiscent of plastic zones in an elastic–plastic body. As the loading is further increased, the lobes close to the hole grow and develop into crossing bands (Fig. 8-2). Finally, we did not observe any significant residual stress in the vicinity of the hole on unloading.

3.3.2. Surface feature: notch

Dog-bone specimens oriented along the rolling axis were prepared with an elliptical notch (3 mm high and 1 mm) wide along one edge but centered along the gage length. Low- and high-magnification observations were made as before, and the results are reported on two specimens so that both low- and high-resolution observations in Fig. 9 correspond to virgin specimens. The macroscopic stress–strain behavior is similar to that observed earlier. As expected, we see larger strains in the immediate vicinity of the notch, and two symmetrically oriented bands of localized strain nucleate from there. Once again, the strains in these bands are less than the fully saturated values when these bands first form, and gradually increase with increasing loading. The bands also increase in size. As the loading continues to increase, other bands oriented approximately 55° to the loading axis form in the regular portions of the gage section. The high-resolution images show that a kidney-shaped region of increased strain develops and begins to grow (Fig. 9-1, 2), eventually developing into the macroscopic bands. Finally, we did not observe any significant residual stress in the vicinity of the notch on unloading.

4. Discussion

The experimental observations presented in the previous section provide various insights into the mechanism of deformation and stress-induced transformation in rolled sheets of nickel–titanium.

The specimens we tested were in the austenite state at room temperature, and initially responded linearly on loading. The departure from linearity began around 1% macroscopic strain as shown in Figs. 3 and 5. We interpret this as the beginning of the phase transformation in the specimen from the austenitic to the martensitic state. However, this departure from linearity was not accompanied by the formation of any localized band of deformation, but by

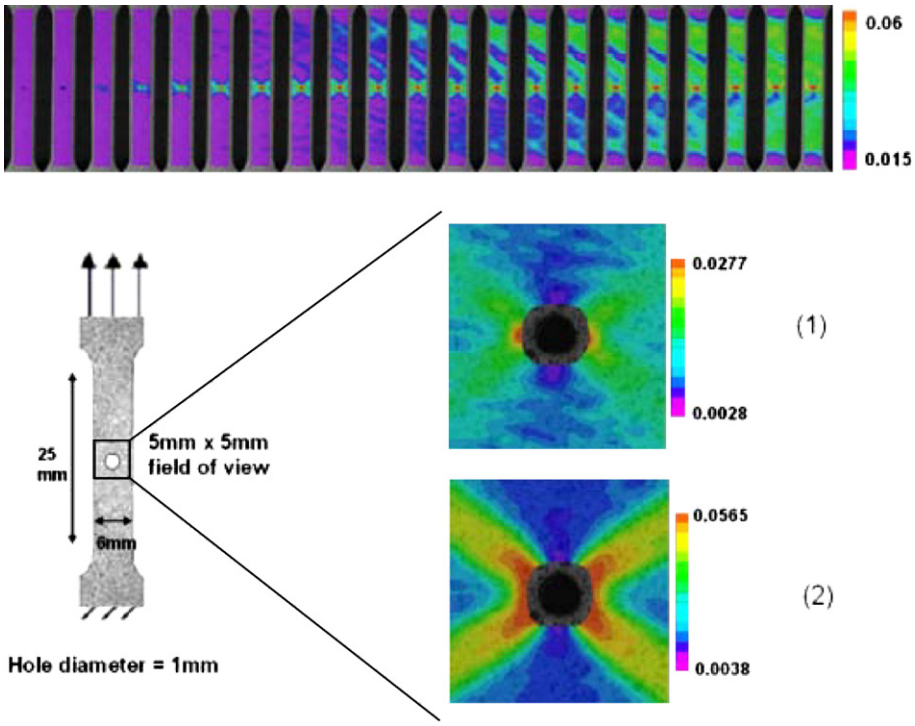

Fig. 8. Strain localization in a non-homogeneous stress field: hole. Panels 1 and 2 show the development of kidney-shaped lobes, which grow and develop into crossing bands as the strain continues to increase. The pictures are shown at different resolutions in order to capture the development of the strain. The top picture shows a snapshot full-field progression of band localization.

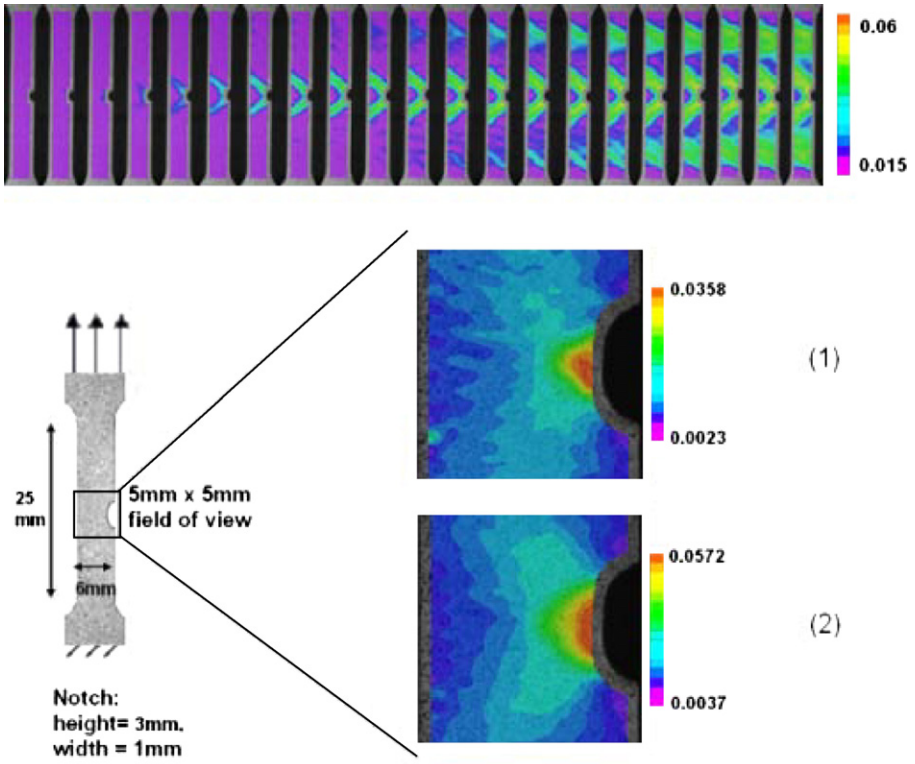

Fig. 9. Strain localization in a non-homogeneous stress field: notch. Panels 1 and 2 show the development of lobes around the notch, which grow and develop into two symmetrically oriented bands as the strain increases. The pictures are shown at different resolutions in order to capture the development of the strain. The top picture shows a snapshot full-field progression of band localization.

almost uniform strain (Fig. 3). This leads us to conclude that the transformation begins homogeneously on a macroscopic scale throughout the specimen without any localization. Ravi-Chandar et al. [13] have reached the same conclusion based on dynamic loading of shape-memory strips.

At the same time, Fig. 3 clearly shows that the strain is not perfectly uniform throughout the specimen but shows some spatial variation. This leads us to conclude that the transformation is microscopically heterogeneous. These conclusions are also supported by the recent experimental observations of Brinson et al. [8], who performed tensile tests of small specimens extracted from sheets while observing the specimen in situ with an optical microscope. They observed that the transformation initiates in small regions inside isolated grains. Our conclusions are also supported by the observations of Barney and Mehta [14], who examined a tensile specimen extracted from a flattened tube using micro-diffraction of synchrotron radiation. Their technique gives a grain-by-grain map of the strain, and their results show that the transformation begins in isolated grains.

The small oscillations in the strain field eventually lead to the formation of localized bands of large strain. Importantly, the strain in the bands is not equal to the saturation value of the transformation strain and we conclude that the transformation does not proceed to saturation inside the bands. Instead the transformation is only partially complete when the bands form and continues with further loading. These observations are consistent with those of Schmahl et al. [9], who also studied rolled sheets using synchrotron radiation. They found that regions inside the deformation band contained significant portions of strained austenite. Furthermore, reorientation of the martensitic variants can also contribute to increasing strain.

As the bands coalesce and the stress begins to rise following the plateau, the transformation begins to saturate. However, we notice that the modulus on loading is noticably smaller than the modulus on unloading in this region. This suggests that the transformation is not complete in this apparently saturated region and one still has residual pockets of austenite which continue to transform with increasing loading. The small modulus on loading is a reflection of this. This is consistent with the microscopic observations of Brinson et al. [8] and Schmahl et al. [9].

Our results also show that geometric defects that cause stress enhancement, such as grips, notches and holes, promote localization. However, localization can also occur in uniform regions of the gage section. This leads us to conclude that localization in SMAs is not a purely geometric instability, but a competition between material and geometric instabilities.

Putting all of these together leads to the following scenario. As we begin to load the austenite, the transformation begins inside isolated grains that are oriented preferentially with respect to the applied stress. These grains are distributed homogeneously on a larger scale, and therefore the transformation initiates homogeneously on the macroscopic scale (much larger than grain size) but heterogeneously on the microscopic scale (comparable to the grain size). This gives rise to an inhomogeneous stress state on the microscopic scale. A combination of these and geometric stress raisers initiate localization. This is resisted by two factors. The first is intergranular constraint. The second is the latent heat that is released, which raises the temperature and the stress required for further transformation and impedes progress of the transformation. Thus, the transformation is not complete even in the bands but requires increasing stress to sustain. Further, the increased latent heat can arrest the development of the bands [5,6], which provides the opportunity for other bands to nucleate and grow. Finally, as the bands coalesce, the transformation is arrested by intergranular constraints and can only proceed by increasing the applied load.

In short, the transformation initiates in well-oriented grains and is saturated by the constraints imposed by the poorly oriented grains. The former is consistent with the observation that the Sachs model, which assumes that each grain deforms independently in response to the uniform applied stress with no regard to the constraint imposed by its neighbors, is a good predictor of the stress at initiation [17]. The latter is consistent with the observation that the Taylor model, which assumes that intergranular constraints are so strong that the mesoscale deformation is uniform, is a good predictor of the transformation strain [18,19]. A synthesis of these two ideas is inherent in the heuristic network model of Novak and Sittner [20] and the mathematical analysis of Schlömerkemper and Bhattacharya [21].

The fact that the initiation and saturation are controlled by two different aspects has important consequences. Schlömerkemper [22] has pointed out that the Sachs and Taylor models gives rise to transformation surfaces that differ dramatically in their eccentricity. This means that the transformation can initiate in one strain direction but saturate in another. This change of strain direction with increasing stress may provide a material mechanism for localization. This implies that texture and crystallography are important factors in determining the propensity of a material to localize. A similar point has been argued by Sittner et al. [11].

Further, it means that one cannot use the resolved stress criterion or the Clausius–Clapeyron relation to predict the onset of transformation. Such a criterion is widely used to predict the onset of various deformation modes, and has been shown to be reasonably accurate for stress-induced transformation of single crystals by Miyazaki [23], Shield [4] and others. In this criterion, it is assumed that the transformation begins when the component of applied stress in the direction of transformation strain reaches a critical value that depends on temperature and latent heat:

$$\sigma \cdot \varepsilon_{\mathrm{T}} = L(T - T_{\mathrm{c}}) \tag{1}$$

where σ is the macroscopic initiation stress, ε_T is the transformation strain, L is the latent heat, T the temperature and T_c the transformation temperature. In our case of uniaxial tension and constant temperature, Eq. (1) becomes simply:

$$\sigma_T \varepsilon_T = C \tag{2}$$

where σ_T is the uniaxial transformation initiation stress, ε_T is the uniaxial transformation strain and C is a constant independent of the orientation. We can easily verify from the data presented in Fig. 6 that this equation does not hold. To elaborate, it follows from Eq. (2) that

$$\frac{\sigma_T(\theta = 0^\circ)}{\sigma_T(\theta = 90^\circ)} = \frac{\epsilon_T(\theta = 0^\circ)}{\epsilon_T(\theta = 90^\circ)}. \tag{3}$$

The experimental data, however, show that

$$\frac{\sigma_T(\theta = 0^\circ)}{\sigma_T(\theta = 90^\circ)} \approx 0.89 \neq \frac{\epsilon(\theta = 0^\circ)}{\epsilon(\theta = 90^\circ)} \approx 1.46 \tag{4}$$

in contradiction of the resolved stress criterion or Clausius–Clapeyron relation.

We finally comment on the finger-shaped localization observed at low values of applied macroscopic strain in the notched specimen. Since the notch is cut asymmetrically, the gage section in the vicinity of the notch is subjected to bending deformation. In other words, the side with the notch has higher compliance and elongates more than the side without the notch. Thus the extensional strain has to decrease as one goes from the side with the notch to the other, and the material accomplishes this using the strain fingers. In this regard, these are the polycrystalline analogs of the tapered twins that have been observed in single crystals subjected to bending [24]. Further, they also show the propensity of the material to have localized deformation at this mesoscale.

5. Conclusions

We have used DIC to study the quantitative full-field strain maps of thin sheets of nickel–titanium subjected to quasistatic uniaxial tension. We have observed strain localization consistent with the work of other researchers, and for the first time have been able to probe its development in terms of strain. This has revealed a much more complex mechanism than assumed in the literature. We find that the transformation initiates in a macroscopically homogeneous but microscopically heterogeneous manner. The transformation proceeds through the nucleation and growth of localized bands of high strain. However, the strain within the bands at formation is significantly smaller than the value at saturation, and gradually increases as the band grows. The transformation is not complete even on apparent saturation of the stress–strain curve. The stress–strain behavior shows a dependence on orientation with respect to the rolling axis, consistent with its texture. We find that the commonly used resolved stress criterion or Clausius–Clapeyron relation does not hold. We have probed the role of geometric defects and shown that localization in SMAs is not purely a geometric instability, but a competition between material and geometric instabilities.

Acknowledgements

We gratefully acknowledge the support of the Army Research Office (W911NF-O4-1-0156), the National Science Foundation (DMS-0311788) and the Powell Foundation. It is a pleasure to acknowledge the suggestions and assistance we received from Professor Daniel Rittel of the Technion during his visits to Caltech throughout this work, as well as the technical expertise and experimental suggestions of Petros Arakelian throughout this project. We gratefully acknowledge Correlated Solutions, Inc. for providing the DIC correlation software used in these experiments.

References

[1] Otsuka K, Wayman CM. Mechanism of shape memory effect and superelasticity. In: Otsuka K, Wayman CM, editors. Shape memory materials. Cambridge: Cambridge University Press; 1998.
[2] Bhattacharya K. Microstructure of martensite: why it forms and how it gives rise to the shape-memory effect. Oxford: Oxford University Press; 2004.
[4] Shield TW. J Mech Phys Solids 1995;43(6):869–95.
[5] Leo PH, Shield TW, Bruno OP. Acta Mater 1993;41(8):2477–85.
[6] Shaw JA, Kyriakides S. J Mech Phys Solids 1995;43:1243–81.
[7] Shaw JA, Kyriakides S. Acta Metall 1997;45(2):683–700.
[8] Brinson LC, Schmidt I, Lammering R. J Mech Phys Solids 2004;52(7):1549–71.
[9] Schmahl WW, Khalil-Allafi J, Hasse B, Wagner M, Heckmann A, Somsen C. Mater Sci Eng A 2004;378(1–2):81–5.
[10] Pieczyska EA, Gadaj SP, Nowacki WK, Tobushi H. Bull Pol Acad Sci Tech Sci 2004;52(3):165–71.
[11] Sittner P, Liu Y, Novak V. J Mech Phys Solids 2005;53(8):1719–46.
[12] Feng P, Sun QP. J Mech Phys Solids 2006;54(8):1568–603.
[13] Niemczura J, Ravi-Chandar K. J Mech Phys Solids 2006;54:2136–61.
[14] Barney M, Mehta A. Private communication.
[15] Sutton MA, Cheng MQ, Peters WH, Chao YJ, McNeill SR. Img Vis Comp 1986;4(3):143–51.
[16] Shabalovskaya SA, Anderegg J, Laab F, Thiel PA, Rondelli G. J Biomed Mater Res B 2003;65(1):193–203.
[17] Sittner P, Novak V. Int J Plast 2000;16:1243–68.
[18] Bhattacharya K, Kohn RV. Acta Mater 1996;44(2):529–42.
[19] Shu YC, Bhattacharya K. Acta Mater 1998;46(15):5457–73.
[20] Novak V, Sittner P. Scripta Mater 2004;50:199–206.
[21] Bhattacharya K, Schlömerkemper A. J Phys 2004;115:155–62.
[22] Schlömerkemper A. PAMM Proc Appl Math Mech, submitted.
[23] Miyazaki S, Kimura S, Takei F, Muira T, Otsuka K, Suzuki Y. Scripta Mater 1983;17:1057–63.
[24] Chopra HD, Bailly C, Wuttig M. Acta Mater 1996;44:747–51.